scientific reports

Check for updates

OPEN

Mitochondrial proteomics reveals reductive metabolism dependent on glutamine in fibroblasts of idiopathic pulmonary fibrosis under hypoxia

Yair Romero[1,15], Manuel Castillejos-López[2,15], Erika Rubí Luis-Garcia[3,15], Adriana Becerra-Cervera[4,5], Diana I. Aparicio-Bautista[4,5], Iliana Herrera[6], Víctor Ruiz[7], Emmanuel Ríos-Castro[8], Carina Becerril[3], Nayeli Torres-Ramírez[1], Rosario Ortiz-Hernández[1], Jose Cisneros[6], Ana Karen Torres-Soria[7], Joaquin Zuñiga[9], Edgar Flores-Soto[10], Yalbi Itzel Balderas-Martinez[11], Ángeles Carlos-Reyes[12], Luz María Torres-Espíndola[13], Rafael Velázquez-Cruz[4]✉ & Arnoldo Aquino-Gálvez[7,14]✉

Pulmonary fibrosis, particularly idiopathic pulmonary fibrosis (IPF), is a chronic disease characterized not only by a transcriptionally active signature associated with hypoxia but also by feedback loops that may underlie disease progression. IPF fibroblasts are known to contribute to disease by the pronounced differentiation of fibroblasts into myofibroblasts, which results in the accumulation of excessive extracellular matrix, creating a hypoxic microenvironment that supports the characteristic phenotype observed in the fibroblasts of these patients. Although several changes have been linked to fibroblast metabolism, the hypoxic conditions in mitochondria generally go unreported. This study aimed to characterize the differences in the mitochondrial proteomic profile between healthy lung fibroblasts and those affected by IPF under hypoxic conditions. We isolated mitochondria and validated the extraction of mitochondrial proteins using electron microscopy and western blotting. Subsequently, we performed label free proteomic analysis to obtain a proteomic profile and validated. Our results revealed that in controls, there is a metabolism of fatty acids and acetyl-CoA regulation, with a slight increase in mitophagy to utilize different substrates as energy sources in an appropriate response to low oxygen conditions. On the other hand, the mitochondria of fibroblasts from patients with IPF show a particular adaptation in glutamine metabolism, which may participate in its commitment to myofibroblast differentiation and the alteration in collagen production. These results allow us to visualize the importance of the proteins that we found deregulated or altered in the mitochondrial context. This helps us to have a basis for future research on their function and possible participation in specific biological processes, especially in the fibrotic process.

Keywords IPF, Mitochondria, Lung fibroblasts, Proteome

Abbreviations

IPF	Idiopathic pulmonary fibrosis
ECM	Extracellular matrix
UIP	Usual interstitial pneumonia
HIF	Hypoxia-inducible factor
INER	National institute of respiratory diseases ismael cosío villegas
ATCC	American type culture collection
LC–MS	Liquid chromatography coupled with mass spectrometry
DEPs	Differentially expressed proteins
PCA	Principal component analysis

[1]Facultad de Ciencias, Universidad Nacional Autónoma de México (UNAM), 04510 Mexico City, Mexico. [2]Laboratorio de Investigación en Epidemiología e Infectología, Instituto Nacional de Enfermedades Respiratorias Ismael Cosío

Villegas (INER), 14080 Mexico City, Mexico. [3]Laboratorio de Biología Celular, Departamento de Fibrosis Pulmonar, Instituto Nacional de Enfermedades Respiratorias Ismael Cosío Villegas (INER), 14080 Mexico City, Mexico. [4]Laboratorio de Genómica del Metabolismo Óseo, Instituto Nacional de Medicina Genómica (INMEGEN), 14610 Mexico City, Mexico. [5]Secretaría de Ciencia, Humanidades, Tecnología e Innovación (SECIHTI), Mexico City, Mexico , 03940 Mexico City, Mexico. [6]Laboratorio de Biopatología Pulmonar INER-Ciencias y Departamento de Investigación en Fibrosis Pulmonar, Instituto Nacional de Enfermedades Respiratorias Ismael Cosío Villegas (INER), 14080 Mexico City, Mexico. [7]Laboratorio de Biología Molecular, Departamento de Fibrosis Pulmonar, Instituto Nacional de Enfermedades Respiratorias Ismael Cosío Villegas (INER), 14080 Mexico City, Mexico. [8]Unidad de Genómica, Proteómica y Metabolómica (UGPM), LaNSE, Cinvestav-IPN, Av. Instituto Politécnico Nacional 2508, San Pedro Zacatenco, Gustavo A. Madero, 07360 Mexico City, MX, Mexico. [9]Laboratorio de Inmunobiología y Genética, Instituto Nacional de Enfermedades Respiratorias Ismael Cosío Villegas (INER), 14080 Mexico City, Mexico. [10]Departamento de Farmacología, Facultad de Medicina, Universidad Nacional Autónoma de México (UNAM), 04510 Mexico City, Mexico. [11]Laboratorio de Biología Computacional, Instituto Nacional de Enfermedades Respiratorias Ismael Cosío Villegas (INER), 14080 Mexico City, Mexico. [12]Departamento de Enfermedades Crónico-Degenerativas, Laboratorio de Onco-Inmunobiología, Instituto Nacional de Enfermedades Respiratorias Ismael Cosio Villegas (INER), 14080 Mexico City, Mexico. [13]Laboratorio de Farmacología, Instituto Nacional de Pediatría (INP), 04530 Mexico City, Mexico. [14]Departamento de Bioquímica, Facultad de Medicina, Universidad Nacional Autónoma de México (UNAM), 04510 Mexico City, Mexico. [15]Yair Romero, Manuel Castillejos-López and Erika Rubí Luis-Garcia contributed equally to this work. ✉email: rvelazquez@inmegen.gob.mx; araquiga@yahoo.com.mx

As is widely known, idiopathic pulmonary fibrosis (IPF) is a progressive, irreversible, and lethal disease, which generally leads to death three to five years after diagnosis and the appearance of initial symptoms. Its pathophysiology is characterized by damage and activation of the alveolar epithelium, proliferation of fibroblasts/myofibroblasts, and exacerbated deposition of the extracellular matrix (ECM), resulting in gradual disorganization and destruction of the lung architecture[1,2]. IPF is considered the most aggressive prototype among interstitial lung diseases due to the progression of its symptoms and its association with the manifestation of a histopathological pattern known as usual interstitial pneumonia (UIP)[3].

The connection between hypoxia and IPF involves several intricate pathophysiological mechanisms. The relationship between hypoxia and IPF involves several complex pathophysiological mechanisms. In IPF patients, the accumulation of fibrotic tissue may lead to some degree of hypoxia, which most likely triggers cellular and molecular responses that help promote fibroblast proliferation and excessive extracellular matrix deposition[4]. We consider that this positive feedback loop may further exacerbate fibrotic disease, leading to its progression[5].

On the other hand, it is known that hypoxia influences the signaling pathways of a hypoxia-inducible transcription factor (HIF), which can regulate the expression of genes involved in pulmonary fibrosis and plays an essential role in the adaptation to metabolic changes in cells. We have observed that HIFs are altered in patients with IPF lung tissue. This leads us to propose that it plays a vital role in altered metabolic processes and the possible involvement of mitochondrial reprogramming or dysfunction.

Therefore, our study aimed primarily to elucidate the role of cellular hypoxia on mitochondria in fibroblasts derived from IPF patients, particularly by examining its relationship with disease development and metabolic changes. Our observations have led us to hypothesize that fibroblasts from IPF patients exhibit mitochondrial adaptation to hypoxia. To explore this hypothesis, we extracted mitochondria from these fibroblasts and performed proteomic analysis, revealing insights into the metabolic adaptations in a fibrotic microenvironment.

Experimental procedures

Human lung fibroblasts

This study was approved by all institutional research committees, including the ethics committee of the National Institute of Respiratory Diseases Cosío Villegas (INER No. B02-19). All methods were carried out in accordance with relevant guidelines and regulations. Two lines of healthy human lung fibroblasts (CCL-201™, CCL-204TM) and two lines of fibroblasts from patients (CCL-134™, CCL-191™) were purchased from American Type Culture Collection (ATCC), and therefore, informed consent was not required for their use. For the primary line obtained from a patient with IPF (Table 1), a waiver of informed consent was obtained and approved by the ethics committee of the National Institute of Respiratory Diseases Cosío Villegas. The cells were cultured in DMEM medium supplemented with penicillin (100U/mL), streptomycin (100 mg/mL), and 10% fetal bovine serum (FBS). The cell cultures were maintained in a humidified atmosphere with 95% air and 5% CO2 at 37 °C until reaching 90% confluence. The cells were proliferated to obtain 1×10^7 fibroblasts were used to isolate the mitochondrial fraction from each experimental group, the lines used reached passages 7–8.

Experimental design

This study investigated the impact of hypoxia on mitochondrial function in lung fibroblasts derived from healthy individuals and patients with IPF. Two variables were considered: disease (healthy vs. IPF) and oxygenation condition (normoxia vs. hypoxia for 72 h). Lung fibroblasts were cultured until reaching sufficient confluency, and 2×10^7 cells were used for each experimental condition. Proteomic analysis of mitochondrial fractions was performed using liquid chromatography coupled to high-resolution mass spectrometry (LC-HRMS). All experiments were conducted in duplicate to ensure reproducibility and robustness of the results.

Hypoxia

To perform the study under hypoxic conditions, fibroblast culture plates were transferred to a modular incubation chamber (Billups-Rothenberg Inc., CA.), where they were maintained at 37 °C for 72 h in a humidified atmosphere with a hypoxemic gas mixture composed of 1% oxygen, 5% CO_2 and the remainder

equilibrated with Nitrogen. The atmosphere composition was monitored using an oxygen analyzer (Teledyne Electronic Technologies 60 T) and an oxygen sensor (OOM105 from EnviteC-Wismar GmbH), following the methods described in previous studies[6].

Isolation of mitochondria
As previously described, the mitochondrial and cytosolic fractions were isolated in fibroblast cultures using the mitochondrial isolation kit for cultured cells (Thermo Scientific 89,874)[7]. For each experimental condition, 2 × 10^7 fibroblasts were used. We employed a reagent-based method in this assay, followed by differential centrifugation to separate the fractions. The mitochondrial and cytosolic fractions were utilized for analysis by Western blotting. The mitochondrial pellet was lysed with 100 µl of 2% CHAPS in Tris-buffered saline (TBS; 25 mM Tris, 0.15 M NaCl; pH 7.2), and the sample was subsequently used for proteomic analysis. Mitochondrial protein content was determined using the Pierce BCA Protein Assay Kit (Product No. 23225).

Electron microscopy
Mitochondria fraction was fixed for 96 h with 2.5% glutaraldehyde, rinsed in phosphate buffer saline (PBS), and postfixed in 1% osmium tetroxide. Next, samples were rinsed in PBS and dehydrated in a graded series of ethanol solutions. Later, mitochondria were dehydrated for 10 min in a 1:1 mixture of alcohol and acetone and twice for 5 min each in acetone. After dehydration, samples were infiltrated overnight in 2:1, 1:1, and 1:2 mixtures of acetone and Durcupan™ ACM resin (Sigma -Aldrich, Darmstadt, Germany). Finally, mitochondria were embedded in Durcupan™ ACM resin. Ultrathin sections were obtained, stained with 4% uranyl acetate and 0.35% lead citrate, and observed under a JEOL 1010 transmission electron microscope. Digital images were taken with a Hamamatsu camera.

Western blot analysis
Proteins were resolved using sodium dodecyl-sulfate polyacrylamide gel electrophoresis (Bio-Rad, Hercules, CA, USA). Briefly, gels loaded with 10 or 15 µg of the protein by lane and run at 150 V were transferred onto a nitrocellulose membrane. The nitrocellulose membranes were incubated on buffer-tris-buffered saline (TBS) and subsequently blocked with 5% skim milk for one hour. Membranes were incubated overnight at 4°C or one hour at room temperature with the primary antibodies: anti-histone H3 (1:1,000), (Thermo Fisher PA5-16,183); anti-VDAC1 (1:100), (Santa Cruz Biotechnology, sc-390996); anti-triosephosphate isomerase (1:5,000), (Abcam ab170894); anti-COX IV (1:2,000), (Abcam ab202554) Glutaminase (1:1000), (Invitrogene, PA5-35,365). The secondary antibodies used were HRP-conjugated substrates anti-mouse (1:10,000) or anti-rabbit (1:2500). Blot images were captured using an Imagen system ChemiDoc (Bio-Rad, Hercules, CA, USA) and analyzed quantitatively using ImageJ software (NIH). The uncropped blots of all Western blots are provided in the Supplementary Figure.

Immunofluorescence
Fibroblasts (control and IPF) were cultured on Lab-tek Chamber slide under normoxic or hypoxic conditions. Cells were fixed with 4% paraformaldehyde for 15 min, permeabilized with 0.1% Triton X-100, and blocked with 5% BSA for 1 h at room temperature. Primary antibodies against α-SMA (Sigma, A2547) and Ki67 ABclonal, A20018) were incubated overnight at 4 °C. After washing, cells were incubated with secondary antibodies conjugated to appropriate fluorophores for 1 h at room temperature. Slides were mounted with antifade mounting medium, and images were acquired using an Olympus IX-81 fluorescence microscope.

Determination of normalizing mitochondrial protein

The mitochondrial fraction and total cell lysate were analyzed using Western blot. Total cell lysates from healthy and IPF lung fibroblasts were prepared with RIPA extraction buffer and protease inhibitors. Protein concentration was quantified using the Bradford colorimetric method. Ten micrograms of mitochondrial protein were loaded and separated on 12% SDS–polyacrylamide gels for the separating gel and 4% for the concentrating gel at room temperature, running the gels at 150 V for 1.5 h. Nitrocellulose membranes were transferred using a wet transfer system at 100 V for one hour. Membranes were blocked with 5% skimmed milk solution for one hour at room temperature. Primary antibodies (anti-COX IV at 1:1,000 and anti-VDAC-1 at 1:100) were then incubated overnight at 4 °C. Secondary antibodies (anti-mouse at 1:10,000 for both primary antibodies) were incubated for one hour at room temperature.

	ID	Type	Age
Healthy	CCD-8, CCL-201™	Cell line	48
	CCD-16, CCL-204™	Cell line	35
IPF	LL-29, CCL-134™	Cell line	26
	LL-97, CCL-191™	Cell line	48
	IPF-1	Primary	73

Table 1. Cell lines.

Sample preparation for mass spectrometry

The protein resuspended in the buffer TBS with 2% CHAPS was quantified using the 2-D Quant® kit (Cytiva, Marlborough, MA, USA), and 50 µg for each replicate was precipitated using MeOH/Chloroform in a proportion of 4:1 and digested according to Ortega-Lozano et al. 2022[8]. Briefly, the resulting pellets were enzymatically digested using iST Sample Preparation Kit® (PreOmics, Munich, GER); 50 µL of "Lyse" reagent was added to protein pellets, placed in a heating block (Eppendorf, Hamburg, GER) during 10 min, 95 °C at 1000 rpm then, samples were sonicated during 20 cycles using BioRuptor Pico® (Diagenode, Liège, BEL) 30 s ON/30 s OFF per cycle. Protein samples were digested using 50 µL of a Lys-C/Trypsin mix ("Digest" reagent) and heating at 37 °C for three hours. Resulting peptides were cleaned in an iST cartridge using a "Wash 1" buffer to eliminate hydrophobic contaminants ("Wash 1" buffer) and "Wash 2" buffer to eliminate hydrophilic contaminants molecules ("Wash 2" buffer); afterward, peptides were eluted using "Elute" reagent and subsequently evaporated to dryness in a SpeedVac (Thermo Fisher Scientific, Waltham, USA), then, peptides were resuspended with "LC-Load" reagent and a aliquot of alcohol dehydrogenase 1 (ADH1) from *Saccharomyces cerevisiae* (Uniprot, accession number P00330; 1 pmol/µl) was added as internal standard to each sample to obtain a final concentration of 25 fmol/µL. The samples were stored at -80 °C until Liquid Chromatography coupled to Mass Spectrometry (LC–MS) analysis.

Mass spectrometry-based proteomics

LC–MS analytical method was applied according to *Ríos-Castro* et al., *2020* with some modifications[9]. Briefly, tryptic peptides were loaded and separated on an HSS T3 C18 column (Waters, Milford, MA); 75 µm × 150 mm, 100 Å pore size, 1.8 µm particle size; using a UPLC ACQUITY M-Class with mobile phase A, 0.1% formic acid (FA) in H_2O, and mobile phase B, 0.1% FA in acetonitrile (ACN) under the following gradient: 0 min 7% B, 121.49 min 40% B, 123.15 to 126.46 min 85% B, 129 to 130 min 7% B, at a flow of 400 $nL{\cdot}min^{-1}$ and 45 °C. The spectra data were acquired in a Synapt G2-S*i* mass spectrometer (Waters, Milford, MA) using nanoelectrospray ionization (nanoESI) and ion mobility separation (IM-MS) using data-independent acquisition (DIA) approach through High-Definition Multiplexed MS/MS ($HDMS^E$) mode. For the ionization source, parameters were set with the following values: 2.75 kV in the sampling capillary, 30 V in the sampling cone, 30 V in the source offset, 70 °C for the source temperature, 0.5 bar for the nanoflow gas, and 150 $L{\cdot}h^{-1}$ for the purge gas flow. Two chromatograms (low and high energy chromatograms) were acquired in a positive mode in a range of m/z 50 – 2000 with a scan time of 500 ms. No collision energy was applied to obtain the low-energy chromatograms, while for the high-energy chromatograms, the precursor ions were fragmented in the transfer cell using a collision energy ramp from 19 to 55 eV.

Analysis

The MS and MS/MS measurements contained in the generated *.raw files were analyzed and quantified by Progenesis QI for Proteomics software *v*4.2 powered by the algorithm developed by Li GZ et al.[10] during the database search (Waters, Milford, MA) using a target decoy strategy against a Homo sapiens *.fasta database (obtained from UniProt, UP000005640, 81,791 protein sequences plus ADH1 from *Saccharomyces cerevisiae*, accession number P00330), which was concatenated with the same *.fasta file in the reverse sense[11]. All chromatographic runs containing the peak intensities are automatically aligned and, consequently the intensities are normalized to avoid possible differences in the amount of injected sample then, peak peaking is performed to select peptide ions prior database search[12]; the algorithm uses an ion accounting process; for detection, *.raw files containing three data functions (low energy, high energy, and lock spray) are processed to obtain an aligned inventory of the retention time of the components with the precise m/z ratio of precursor (low energy) and fragment ions (high energy) to complete the ion detection process; subsequently, the filtering is performed to eliminate precursor ions and fragment ions under 750 and 350 Da, respectively. Then, the reversed database (target decoy) is created to classify false positive identifications and additionally, the algorithm produces a fragmentation model by comparing the distribution of the experimental product ions with the number of times and a specific bond cleavage was identified[13]. Finally, the algorithm performs additional comparisons based on the fourteen physicochemical properties of peptides undergoing CID fragmentation[11].

Proteins were reviewed, and the functions "export peptides/protein measurements" were used to generate the output files (*.csv) for subsequent analysis. Only peptides that satisfied the theoretical model of fourteen physicochemical properties were kept at the protein level (https://doi.org/10.1016/j.bbapap.2024.141049). Parameters used for the protein identification were trypsin as cutting enzyme and one missed cleavage allowed; carbamidomethyl (C) as a fixed modification and oxidation (M), amidation (C– terminal), deamidation (Q, N) and phosphorylation (S, T, Y) as variable modifications; default peptide and fragment tolerance (maximum normal distribution of 10 and 20 ppm respectively) and false discovery rate (FDR) ≤ 1%; all false identifications (Reversed proteins) and proteins with one peptide identified were discarded for subsequent analysis. Synapt G2-S*i* was calibrated with [Glu1]-Fibrinopeptide fragments through the precursor ion $[M+2H]^{2+} = 785.84261$ fragmentation of 32 eV at one ppm across all MS/MS measurements. Quantification of proteins was calculated based on the average MS signal response of the three most intense tryptic peptides (Top3)[14] according to the following equations[14–16].

$$Top3 = \sum_{i=1}^{3} PeptideIntensity$$

where the Top3 value is the arithmetic mean of the MS signal response of the three most intense tryptic peptides. Using the Top3 value of the internal standard as well as of interest proteins, it is possible to determine the amount of protein in each sample using the following equation $fmol = \frac{\sum_{i=l}^{3} PeptideIntensityA}{\sum_{i=l}^{3} PeptideIntensityB}(X)$.

where A is the protein of interest, B is the internal standard (ADH1), and "X" is the concentration in fmol/µl of internal standard. Generated *. csv files during the database search were used for subsequent analysis.

Statistical and bioinformatics analysis

Proteome datasets were filtered using the criteria of at least one unique peptide and ≥ 2 peptides. Differentially expressed proteins (DEPs) were determined with a fold change > 1.5 or < 1.5 and p-value < 0.05, using a two-tailed student's t-test or Wilcoxon signed–rank nonparametric test. To examine clustering or separation between conditions, principal component analysis (PCA) was performed and used to visualize variability by cell type (controls and IPF fibroblasts) and by oxygenation condition (normoxia and hypoxia). All plots were performed with R 4.3.0 tools.

Results

Mitochondria isolation from human lung fibroblasts

Mitochondria were isolated from fibroblasts from healthy lungs and IPF patients exposed to 72 h of either normoxia or hypoxia. After, proteomic analysis was done using high-resolution mass spectrometry and liquid chromatography of all experiments in duplicate (Fig. 1). Electron microscopy confirmed the presence of mitochondria, as shown in Fig. 2A; mitochondria isolated from lung fibroblasts exhibit few and widened cristae despite being derived from healthy patients, suggesting isolation artifacts. After assessing the amount of mitochondrial material sufficient to justify continuing the process despite the impurities detected, the decision was made to proceed with proteomic analysis. In addition, to confirm the correct separation of the mitochondrial fraction, we performed an immunoblot of the different isolated fractions (cytoplasm, mitochondria, and total lysate). Specific markers were used for each fraction, and it was observed that the mitochondria fraction was correctly purified Fig. 2B. Therefore, the impurities could be due, at least in part, to mitochondrial content from damaged mitochondria during the purification process. Integrity gels were performed for all experimental samples before the proteomic analysis Fig. 2C. Additionally, a western blot was performed using COX IV protein as the mitochondrial load control to demonstrate the same amount of mitochondrial protein Fig. 2D.

Slight variations in the mitochondrial proteome of IPF fibroblasts under hypoxic conditions

We can quantified a total of 1934 proteins, all these protein identifications and parameters such as accession number, number of peptides per proteins, sequence coverage as well as all peptide identifications detailing physicochemical parameters including mass error in ppm, m/z, molecular weight, sequence modifications (including PTM´s) among others are reporting in the *.csv files which are deposited in the PRoteomics IDEntifications Database (PRIDE) (https://doi.org/10.1093/nar/gkae1011) with a repository number PXD064472 then, we filtered the proteins to include those that present at least two or more peptides and at least one unique peptide. To analyze the clustering patterns and detect possible differences among the groups, PCA was used (Fig. 3A,B). Our study identified protein expression differences based on cell type (mitochondrial proteins from control fibroblasts and fibroblasts of patients with IPF) and oxygenation conditions (normoxia and hypoxia). Volcano diagrams display all differentially expressed proteins in the control group (Fig. 3C) and IPF patient fibroblasts (Fig. 3D) under hypoxia. In our analysis, an exclusive focus was placed on mitochondrial proteins. The MitoCarta 3.0 database defined these proteins, including 1,136 verified, associated, and auxiliary human mitochondrial genes (version 2021)[17]. One thousand nine hundred thirty-four proteins were identified,

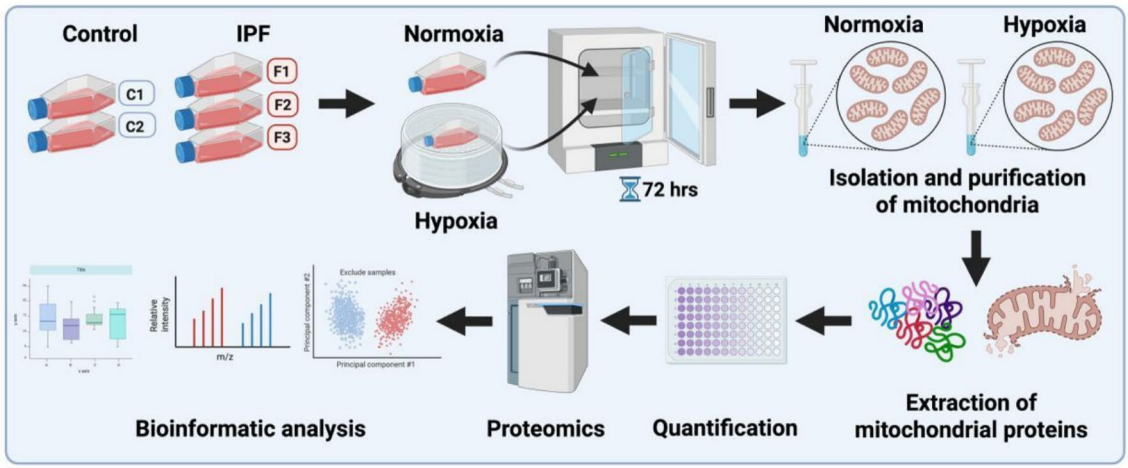

Fig. 1. Study design to analyze the mitochondrial proteome. Created in BioRender.

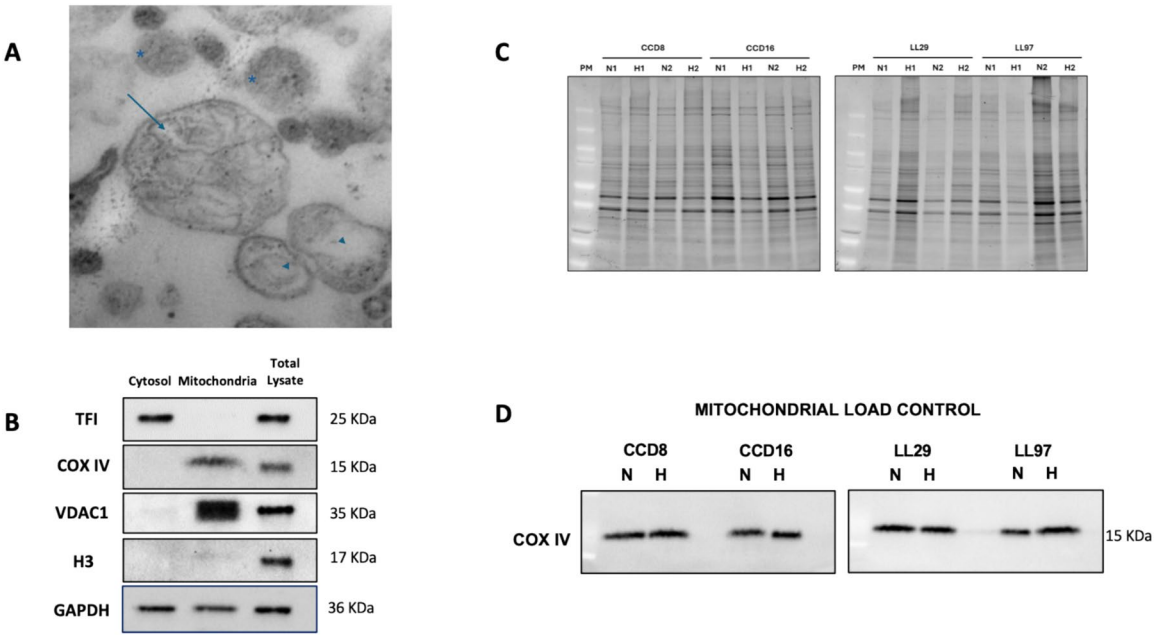

Fig. 2. Mitochondrial fraction isolation. (**A**) Electron microscopy images of mitochondria isolated from lung fibroblasts show inner membrane folds suggestive of opened or widened cristae (arrow). Few cristae with vesicular appearance (head arrow). Possible mitochondria without limiting membrane (*). (**B**) Western blot for triose phosphate isomerase (TPI) as a marker of the cytosol, COX IV, and VDAC1 in the mitochondrial fraction; Histone 3 (H3) as a marker of total lysate only. GAPDH was used as a loading control. (**C**) Electrophoresis protein integrity gels. **D** Mitochondrial load control for each cell line under different oxygenation conditions.

of which 609 were mitochondrial, accounting for 31.4%. A two-way Venn diagram illustrates the unique and shared proteins between groups, showing the overlap and distinct proteins under different conditions (Fig. 3E). In the hypoxic control group, 497 mitochondrial proteins were found, while in the IPF group, 399 were found, with 393 proteins shared between the two. This overlap in proteins indicates similarities in both profiles under hypoxic conditions.

Alternative energy sources and stress adaptation in control fibroblasts under hypoxia

Regarding mitochondrial proteins deregulated in a hypoxic environment, we identified twelve proteins in the control group in hypoxia, of which seven were upregulated and five were downregulated (Table 2). The increase in proteins such as ACSL-3, ACSM-1, and ACAD-8, as observed in Fig. 4A, suggests a metabolic adaptation that may enhance the fibroblasts' ability to utilize fatty acids and alternative substrates for energy production under low oxygen availability. Long-chain acyl-CoA synthetase 3 (ACSL-3) is known to be a key enzyme in fatty acid metabolism, playing a crucial role in activating long-chain fatty acids for cellular lipid synthesis and β-oxidation[18–20]. Similarly, medium-chain acyl-coenzyme A synthetase-1 (ACSM-1) is involved in the first step in fatty acid metabolism by catalyzing the activation of fatty acids by CoA to produce acyl-CoA[21,22]. Isobutyryl-CoA dehydrogenase (ACAD-8) is specifically responsible for valine catabolism, transforming isobutyryl-CoA into methacrylyl-CoA, which is subsequently converted to propionyl-CoA and acetyl-CoA, both of which enter the Krebs cycle[23,24].

On the other hand, increased PHB2, ATP13A2, LGALS3, and VDAC1 indicate an active adaptation of mitochondria to maintain homeostasis and optimize energy production under stress conditions (Fig. 4A). PHB2 plays a significant role in mitophagy, while ATP13A2 is involved in the mitochondrial oxidative stress response. LGALS3 is a protein associated with profibrotic responses, and VDAC1 is involved in hypoxia, fibroblast apoptosis, and fibrosis. On the other hand, the decrease in mitochondrial proteins in healthy lung fibroblasts under hypoxic conditions, such as ACAD10, MYG1, POR, GSTK1, and GRK6, suggests an adaptive response to hypoxia. This could compromise mitochondrial function, energy production, and regulation of oxidative stress (Fig. 4B). ACAD10 is essential for fatty acid oxidation and catabolism of short-chain 4-hydroxy acids and is involved in pexophagy, regulating the removal of damaged peroxisomes[25,26]. The NADPH P450 reductase (POR) serves as an electron donor, furthermore, facilitating the drug metabolism and regulating the reactive oxygen species (ROS) production[27,28]. Glutathione S-transferase kappa 1 (GSTK1) aids in oxidative stress responses and redox signaling, with its expression induced under caloric restriction[29,30]. Inhibition of PGC-1α suppresses GSTK1, increasing ROS accumulation and promoting ferroptosis[31]. GRK6 regulates the STAT3 pathway, which is crucial for cell proliferation[32]. MYG1, a 3'-5' RNA exonuclease, plays a crucial role in mitochondrial function and promotes glycolysis by stabilizing PKM2[33]. These findings emphasize the complex relationship between

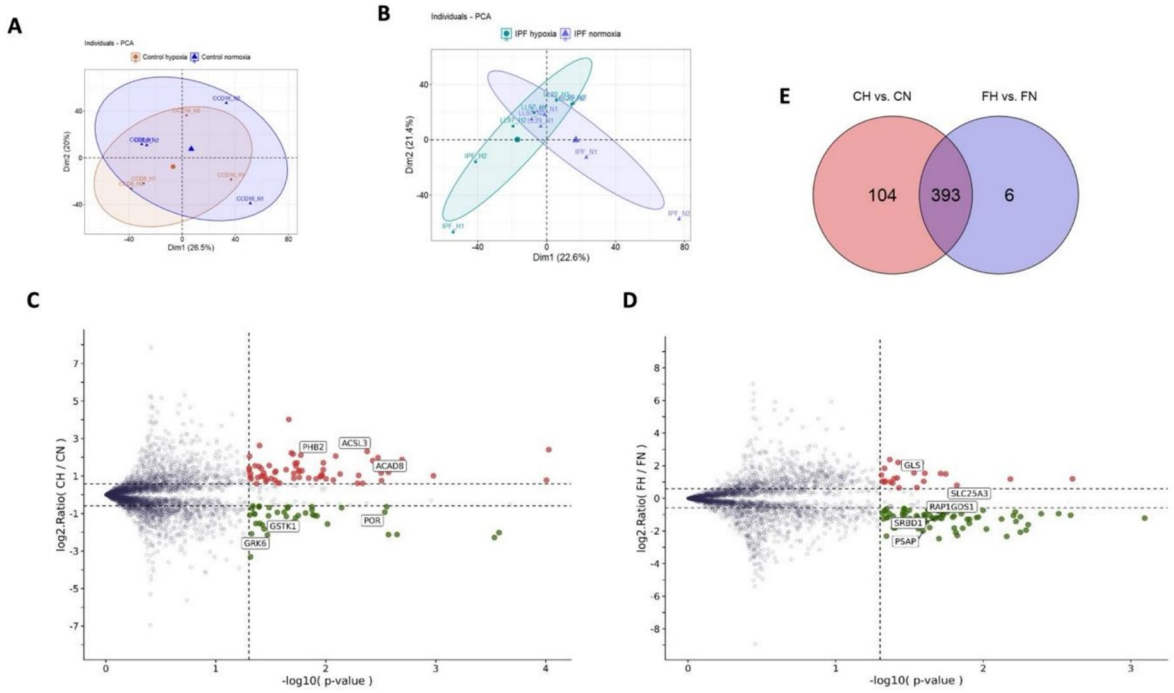

Fig. 3. Analysis of mitochondrial proteome in IPF and controls fibroblasts under hypoxia. (**A**) Principal Component Analysis (PCA) of Control Hypoxia vs. Control Normoxia. (**B**) PCA of IPF Hypoxia vs. IPF Normoxia. Volcano plots show over- and under-expressed proteins in hypoxia for (**C**) healthy controls and (**D**) IPF fibroblasts, upregulated proteins are shown in red dots, and downregulated proteins are shown in green dots. The (**E**) Venn diagram shows differentially expressed mitochondrial proteins in Control Hypoxia vs. Control Normoxia and IPF Hypoxia vs. IPF Normoxia.

Symbol (UniProtKB)	Description	Unique Peptides	log2 Ratio	P value	Max fold chang
ACSL3	Fatty acid CoA ligase	1	2.31	0.004	4.81
PHB2	Prohibitin	1	2.11	0.016	3.52
ACAD8	Isobutyryl-CoA dehydrogenase mitochondrial	1	1.97	0.003	1.57
VDAC1	Voltage-dependent anion-selective channel protein 1	4	1.23	0.017	2.69
ATP13A2	Isoform B of Polyamine-transporting ATPase 13A2	1	0.95	0.011	1.04
LGALS3	Galectin-3	6	0.88	0.014	1.97
ACSM1	Acyl-coenzyme A synthetase ACSM1 mitochondrial	1	0.74	0.003	1.60
ACAD10	Acyl-CoA dehydrogenase family member 10	3	− 0.72	0.046	1.52
MYG1	MYG1 exonuclease	1	− 0.80	0.013	1.53
POR	NADPH-cytochrome P450 reductase	1	− 0.92	0.002	1.48
GSTK1	Glutathione S-transferase kappa 1	4	− 1.23	0.018	3.00
GRK6	G protein-coupled receptor kinase	1	− 2.14	0.033	3.73

Table 2. Differentially expressed proteins in mitochondria of healthy fibroblasts in hypoxia The first column shows the UniProtKB symbol, followed by protein description, unique peptides, log ratio, ANOVA p-value, log 2 ratio, and maximum fold change of mitochondrial proteins in hypoxic control fibroblasts. Negative ANOVA p-values indicate a decrease in protein levels compared to normoxia. A log 2 ratio of + 1 indicates a doubling of protein levels, while -1 indicates halved levels under the experimental condition

hypoxia and the regulation of mitochondrial function in the context of oxidative stress, emphasizing the implications of decreased levels of these proteins.

Hypoxia-induced glutaminolysis in mitochondria of IPF fibroblasts

In Table 3, the hypoxic IPF group shows six identified proteins, two upregulated and four downregulated. As we can observe in Fig. 5A, there is an increase in two proteins called GLS1 and SLC25A3, which indicates that these mitochondria in hypoxia present a characteristic profile of the mitochondrial metabolism of fibroblasts from patients with IPF. We validated these results and observed a diametrically opposite response in fibroblasts

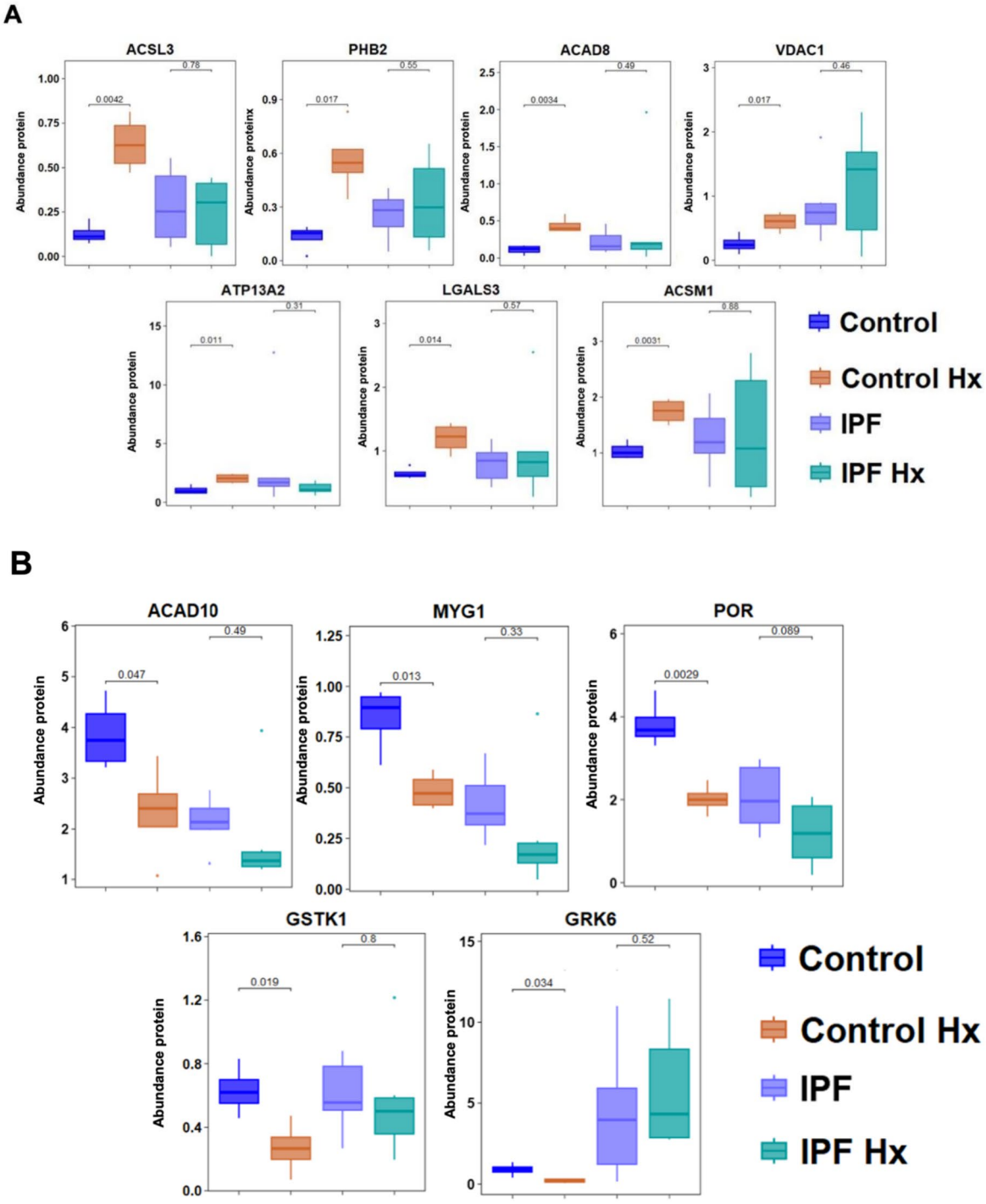

Fig. 4. Differentially expressed mitochondrial proteins in control fibroblasts under hypoxia. (**A**) Increased and (**B**) decreased protein expression in mitochondria. Box plots illustrate the differences in protein expression, highlighting deregulated proteins in normoxia (Control) and hypoxia (Control Hx), represented by blue and orange boxes, respectively. Additionally, the expression of IPF proteins in normoxia (IPF) and hypoxia (IPF Hx) is depicted by purple and green boxes, respectively.

from IPF patients, characterized by upregulation of GLS (Fig. 6A-C) (Supplementary file). This increase could be related to the biochemical process known as reductive carboxylation (RC) of glutamine, where glutamine is converted to α-ketoglutarate by adding a carboxyl group (CO_2) and its reduction by specific enzymes. This process is fundamental for cell metabolism, particularly when intermediates are required in the tricarboxylic acid cycle (TCA). RC is essential for regulating and maintaining energy metabolism and is also used to synthesize compounds necessary for cell proliferation, especially in tumor cells. RC of glutamine is part of the metabolic reprogramming associated with hypoxia-inducible factor 1 alpha (HIF-1α) since constant activation of HIF-1α

Symbol (UniProtKB)	Description	Unique peptides	log2 ratio	P value	Max fold change
GLS	Glutaminase kidney isoform mitochondrial	3	1.53	0.024	2.66
SLC25A3	Phosphate carrier protein mitochondrial	4	0.79	0.015	1.46
MRPL12	39S ribosomal protein L12 mitochondrial	1	− 0.73	0.031	1.52
RAP1GDS1	Isoform 4 of Rap1 GTPase-GDP dissociation stimulator 1	1	− 1.17	0.020	1.48
SRBD1	S1 RNA-binding domain-containing protein 1	1	− 1.26	0.021	5.29
PSAP	Prosaposin	2	− 2.00	0.025	1.08

Table 3. Differentially expressed proteins in mitochondria of IPF fibroblasts in hypoxia The first column shows the UniProtKB symbol, followed by protein description, unique peptides, log ratio, ANOVA p-value, log 2 ratio, and maximum fold change of mitochondrial proteins in IPF hypoxic fibroblasts. Negative ANOVA p-values indicate a decrease in protein levels compared to normoxia. A log 2 ratio of + 1 indicates a doubling of protein levels, while -1 indicates halved levels under the experimental condition.

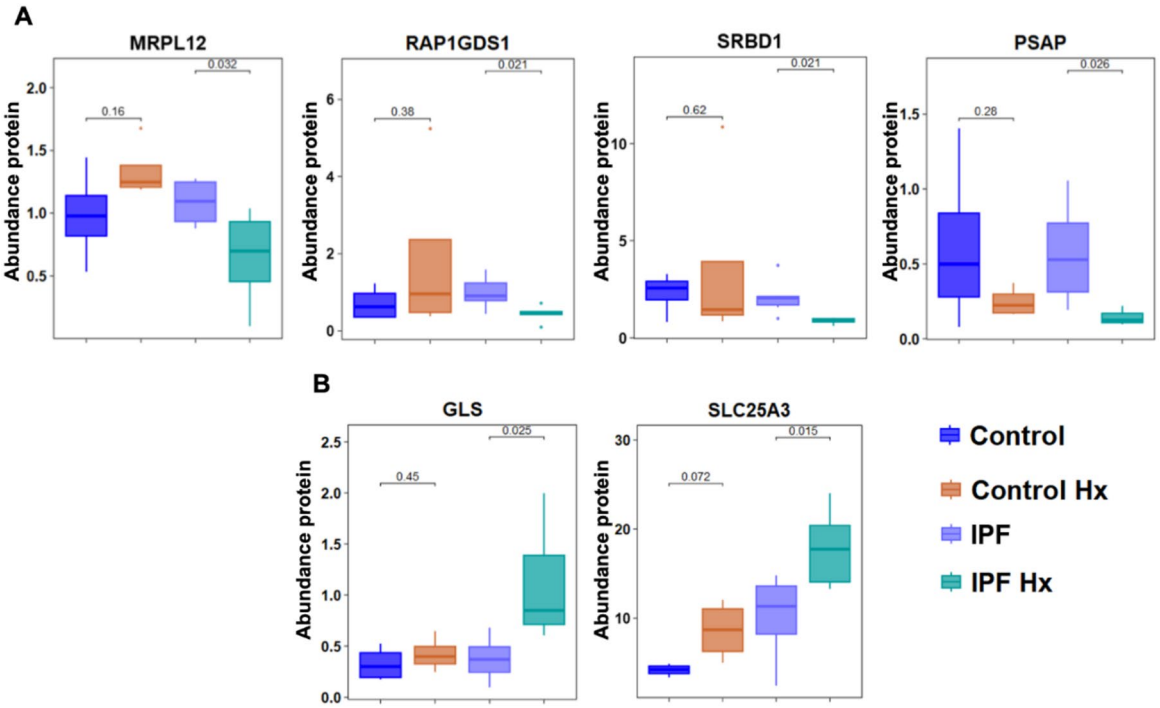

Fig. 5. Differentially expressed mitochondrial proteins in IPF fibroblasts under hypoxia. (**A**) Increased and (**B**) decreased protein expression in mitochondria. Box plots illustrate differences in protein expression, highlighting proteins deregulated in normoxia (Control) and hypoxia (Control Hx), represented by blue and orange boxes, respectively. Additionally, IPF protein expression in normoxia (IPF) and hypoxia (IPF Hx) is represented by purple and green boxes, respectively.

reproduces the preferentially reductive metabolism of glutamine-derived α-ketoglutarate, even under normoxic conditions[34]. Additionally, we assessed the degree of differentiation using α-SMA as a marker for myofibroblasts and Ki67 for proliferation. IPF fibroblasts showed higher baseline levels of α-SMA expression compared to controls. Under hypoxia, both markers increased in both groups, with α-SMA expression remaining higher in IPF fibroblasts, whereas Ki67-positive cells were more prominent in the control group. Notably, Ki67 was absent in highly differentiated cells (Fig. 6D).

Hypoxia induces changes in the mitochondrial metabolism of lung fibroblasts, especially in patients with IPF. An increase in the expression of GLS and SLC25A3 was observed, suggesting a higher activity of glutaminolysis (Fig. 7). Instead of conventional oxidation, we propose that this process could drive collagen synthesis through reductive carboxylation, a mechanism described in tumor cells[35–38]. The decreased oxygen concentration could promote the observed metabolic shift, allowing the fibrotic fibroblasts' mitochondria to adapt to a hypoxic environment and contribute to the fibrotic phenotype[39–42]. On the other hand, and in a contrary sense, proteins such as MRPL12, RAP1GDS1, SRBD1, and PSAP are observed to have decreased expression (Fig. 5B). These proteins are necessary for cell cycle, stress response, and mitochondrial homeostasis maintenance. This indicates that there are alterations in these mechanisms during IPF progression. For example, it has been reported that MRPL12 is essential for mitochondrial function. It binds to the ANT3 protein to stabilize the mitochondrial

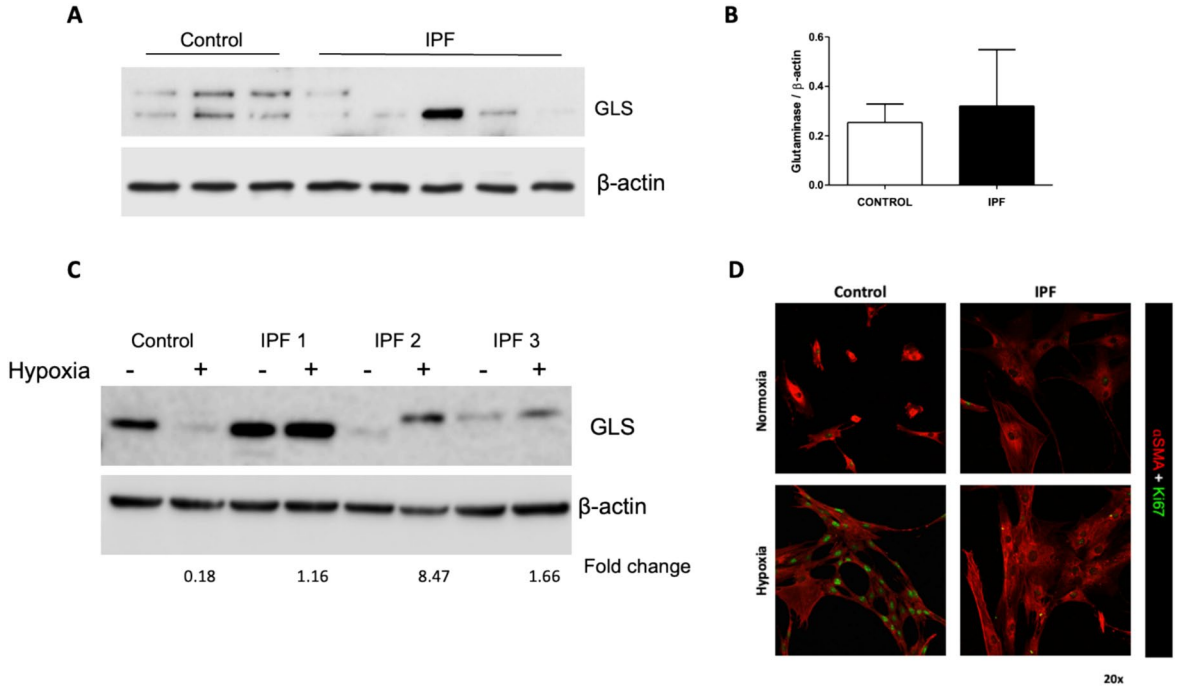

Fig. 6. Validation of the glutaminase response under hypoxic conditions. (**A**) Western blot for GLS in total lysate (Control Normoxia n = 3 and IPF Normoxia n = 5. ® actin was used as a loading control. (**B**) Graph of the densitometric analysis. (**C**) Representative immunoblot of GLS and ® actin was used as a loading Control (normoxia and hypoxia) and IPF 1, 2 and 3 (normoxia and hypoxia). (**D**) Representative images showing the colocalization of α-SMA (red) and Ki67 (green) in control and IPF fibroblasts under normoxic and hypoxic conditions.

membrane and plays a crucial role in oxidative phosphorylation[43,44]. Its downregulation reduces OXPHOS, affects cell growth[45], and regulates protein production and mitochondrial DNA expression[46]. RAP1GDS1 acts as a guanine nucleotide exchange factor (GEF) for GTPases like RHOA, RAC1, and KRAS and helps mitigate statin-induced cardiac hypertrophy and fibrosis by influencing relevant signaling pathways[47–49]. SRBD1, a mitochondrial protein, accumulates in nucleus pulposus cells due to NBR1 reduction, promoting cellular senescence and the SASP phenotype via AKT1/p53 and NF-κB pathways[50]. We must also mention that a saponin precursor glycoprotein essential for lysosome lipid degradation is called prosaposin (PSAP) and is associated with deficiencies linked to lysosomal storage disorders and neurodegenerative diseases[51–54]. These findings underscore the disruptions in mitochondrial and cellular homeostasis that may contribute to the pathophysiology of IPF.

Discussion

Oxygen homeostasis is essential for maintaining lung structure and function; however, in conditions like IPF, dense fibrotic regions of lung often become hypoxic[55]. This localized hypoxia is a hallmark of fibroblast foci in IPF and contributes to disease progression and irreversibility. Consequently, a pathological feedback loop may be established, driven by complex interactions between epithelial cells and fibroblasts, which in turn influence regeneration and pathogenesis. This dynamic motivates us to propose the possible existence of a mitochondrial switch that is reminiscent of and consistent with mechanisms frequently observed in several types of cancer. Understanding the specific changes hypoxia induces in mitochondrial function at the metabolic level is relevant to elucidating the biochemical and molecular mechanisms underlying IPF. Recent work highlights the critical role of mitochondrial dysfunction in developing pulmonary fibrosis, particularly within the alveolar epithelium and fibroblasts. In alveolar type II cells from IPF patients, the accumulation of dysmorphic mitochondria and a deficiency in mitophagy—mediated by reduced PINK1 levels—promote apoptosis and activate profibrotic pathways, exacerbating lung damage[56]. Notably, our previous studies have shown that fibroblasts from IPF patients under normoxic conditions exhibit elevated levels of hypoxia-inducible transcription factors (HIF-1α and HIF-2α), indicating a state of pseudohypoxia and highlighting the importance of the hypoxia signaling pathway in activating fibroblasts and myofibroblasts[57]. Considering the background outlined above, we needed to investigate what metabolic changes occur in the mitochondria of fibroblasts from IPF patients. Therefore, to investigate the mitochondrial proteome in these fibroblasts under low oxygenation conditions, we used a mitochondrial isolation method that, although it did not achieve optimal purity, allowed us to detect significant differences in the mitochondria of control fibroblasts and fibroblasts from patients with IPF. It is worth noting the high similarity in protein expression in response to hypoxia between mitochondria from controls and IPF patients.

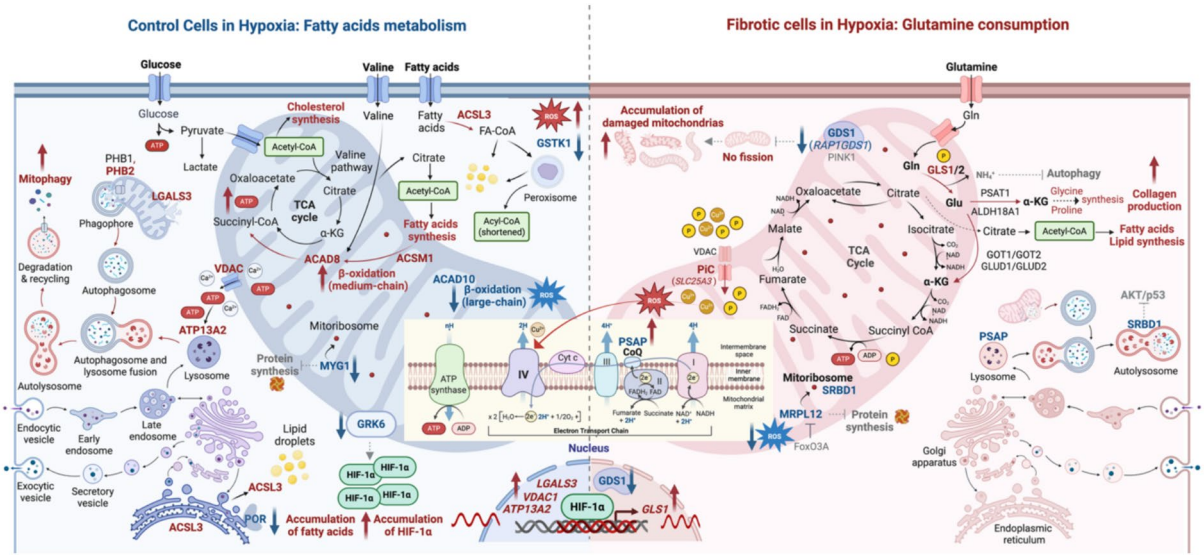

Fig. 7. Summary scheme. This scheme illustrates the deregulated proteins in the mitochondria of control fibroblasts and fibroblasts from IPF patients under hypoxic conditions, emphasizing the metabolic pathways and cellular mechanisms these proteins may influence. The fatty acid metabolic pathway is indicated to be active in hypoxic control fibroblasts (represented by blue mitochondria). At the same time, glutaminolysis is suggested to play a critical role in the mitochondria of IPF fibroblasts (represented by pink mitochondria). Created in BioRender.

Some of these proteins were set aside for future analysis, as our focus was explicitly on general mitochondrial phenomena. As expected, the differentially expressed proteins in controls primarily reorganize metabolism to utilize alternative TCA cycle substrates and stress adaptation, including mitophagy and oxidative response. These results align with studies indicating that IPF fibroblasts tend to consume less oxygen and have a remarkable resistance to apoptosis, which has been linked to alterations in the mitochondrial permeability transition pore (mPTP); these changes decreasing cytochrome c release and ATP production, ultimately improving fibroblast survival in a fibrogenic environment[7]. In this context, increased levels of VDAC-1 are associated with fibroblast activation and a reduction in fatty acid β-oxidation, in fatty acid β-oxidation, suggesting a potential protective role in regulating long-chain fatty acid metabolism[58].

Chronic oxidative stress, often linked to aging, contributes to mitochondrial dysfunction, in this sense it is widely known that the incidence and prevalence of IPF increase significantly with age, making age a critical factor for its progression[59–63]. In the dynamic landscape of reactive oxygen species (ROS) response, these species appear to function as complex signaling mechanisms; it is well established that HIF-α signaling is ROS-dependent and that HIF can regulate its overexpression. This oxidative stress alters normal mitochondrial dynamics in IPF, creating a cycle that promotes the fibrotic phenotype. Studies have shown metabolic alterations in the lungs of IPF patients, including elevated lactate levels and dysregulation of the ROS-generating enzyme NADPH oxidase-4 (Nox4)[64–66]. Similarly, our work shows that ROS chemically oxidizes ACAD10, and NADPH P450 reductase (POR) is an essential electron donor for various enzymes and regulates ROS production, affecting hypoxic responses and gene induction under stress[27,28,67,68]. ATP13A2 has emerged as a critical player in the context of IPF; its decrease correlates with an increase in fibrosis markers, suggesting a link to disease progression[69]. ATP13A2 is vital for polyamine homeostasis and protection against oxidative stress, and loss of function leads to mitochondrial dysfunction[70,71]. Glutathione S-transferase kappa 1 (GSTK1) involved in the response to oxidative stress and is induced in a caloric restriction situation, which helps improve resistance to oxidative stress[29,30]. These findings highlighted significant alterations in mitochondrial dynamics in IPF.

Our results indicate a metabolic dysregulation in IPF fibroblasts, marked by alterations in glutaminolysis and reductive carboxylation. The enhanced GLS-mediated glutaminolysis in lung myofibroblasts is a crucial metabolic adaptation that promotes fibrosis by facilitating collagen production induced by the profibrotic factor TGF-β. This pathway, involving key enzymes such as PSAT1 and ALDH18A1[72,73]; activates mTORC1 signaling, which enhances collagen translation and stability, and also increases α-ketoglutarate (α-KG) levels, further stimulating collagen expression[74]. Although not directly addressed in this study, the potential contribution of reductive carboxylation as a carbon source for collagen synthesis in myofibroblasts warrants further investigation.

Conclusions

Our results demonstrate that hypoxia induces significant mitochondrial reprogramming in healthy lung fibroblasts and those from patients with IPF. In the case of mitochondria from fibroblasts from patients with IPF, reprogramming is consistent with the differentiation of fibroblasts into myofibroblasts and collagen production, all related to the progression of fibrosis. The involvement of glutaminase 1 (GLS1) and the copper transporter SLC25A3 highlights a dysregulation of glutaminolysis and reductive carboxylation pathways in this context.

Data availability

The data supporting the findings of this study are available upon formal request to the corresponding author. Additionally, the raw csv files have been deposited in the PRoteomics IDEntifications Database (PRIDE) under the repository accession number **PXD064472**, available online: 10.6019/PXD064472

Received: 7 July 2025; Accepted: 31 October 2025
Published online: 11 January 2026

References

1. King, T. E., Pardo, A. & Selman, M. M. Idiopathic pulmonary fibrosis. *Lancet* **378**, 1949–1961 (2011).
2. Selman M, TE K, Jr., Pardo A, King J, Pardo A. Idiopathic pulmonary fibrosis: Prevailing and evolving hypotheses about its pathogenesis and implications for therapy. Ann Intern Med. 134:136–51. (2001).
3. Selman, M. & Pardo, A. Idiopathic Pulmonary Fibrosis: From Common Microscopy to Single-Cell Biology and Precision Medicine. *Am. J. Respir. Crit. Care Med.* **209**, 1074–1081 (2024).
4. Tzouvelekis, A. et al. Comparative expression profiling in pulmonary fibrosis suggests a role of hypoxia-inducible factor-1α in disease pathogenesis. *Am. J. Respir. Crit. Care Med.* **176**, 1108–1119 (2007).
5. Romero Y, Aquino-Gálvez A. Hypoxia in Cancer and Fibrosis: Part of the Problem and Part of the Solution. Int J Mol Sci. (2021).
6. Aquino-Gálvez A, González-Ávila G, Jiménez-Sánchez LL, Maldonado-Martínez HA, Cisneros J, Toscano-Marquez F, et al. Dysregulated expression of hypoxia-inducible factors augments myofibroblasts differentiation in idiopathic pulmonary fibrosis. Respir Res. 20. (2019).
7. Luis-García ER, Becerril C, Salgado-Aguayo A, Aparicio-Trejo OE, Romero Y, Flores-Soto E, et al. Mitochondrial Dysfunction and Alterations in Mitochondrial Permeability Transition Pore (mPTP) Contribute to Apoptosis Resistance in Idiopathic Pulmonary Fibrosis Fibroblasts. Int J Mol Sci. 22. (2021).
8. Ortega-Lozano AJ, Jiménez-Uribe AP, Aranda-Rivera AK, Gómez-Caudillo L, Ríos-Castro E, Tapia E, et al. Expression Profiles of Kidney Mitochondrial Proteome during the Progression of the Unilateral Ureteral Obstruction: Focus on Energy Metabolism Adaptions. Metabolites. 12. (2022).
9. Ríos-Castro, E. et al. Quantitative Proteomic Analysis of MARC-145 Cells Infected with a Mexican Porcine Reproductive and Respiratory Syndrome Virus Strain Using a Label-Free Based DIA approach. *J. Am. Soc. Mass Spectrom.* **31**, 1302–1312 (2020).
10. Li, G.-Z. et al. Database searching and accounting of multiplexed precursor and product ion spectra from the data independent analysis of simple and complex peptide mixtures. *Proteomics* **9**, 1696–1719 (2009).
11. Käll, L., Storey, J. D., MacCoss, M. J. & Noble, W. S. Assigning significance to peptides identified by tandem mass spectrometry using decoy databases. *J. Proteome Res.* **7**, 29–34 (2008).
12. Cavuzic MT, de Sousa AS, Lohman JR, Waldrop GL. Kinetic characterization of the C-terminal domain of Malonyl-CoA reductase. Biochimica et Biophysica Acta (BBA) - Proteins and Proteomics. 1872, 141033. (2024).
13. Geromanos, S. J. et al. The detection, correlation, and comparison of peptide precursor and product ions from data independent LC-MS with data dependant LC-MS/MS. *Proteomics* **9**, 1683–1695 (2009).
14. Silva, J. C., Gorenstein, M. V., Li, G.-Z., Vissers, J. P. C. & Geromanos, S. J. Absolute quantification of proteins by LCMSE: a virtue of parallel MS acquisition. *Mol. Cell Proteomics.* **5**, 144–156 (2006).
15. Arnaud-Franco G, Ríos-Castro E, Velasco-Suárez A, García-de León FJ, Beltrán LF, Carbajal-Saucedo A. Venom comparisons of endemic and micro-endemic speckled rattlesnakes Crotalus mitchellii, C. polisi and C. thalassoporus from Baja California Peninsula. Toxicon. 224, 107030. (2023).
16. Barrera-Rojas J, Gurubel-Tun KJ, Ríos-Castro E, López-Méndez MC, Sulbarán-Rangel B. An Initial Proteomic Analysis of Biogas-Related Metabolism of Euryarchaeota Consortia in Sediments from the Santiago River, México. Microorganisms. 11. (2023).
17. Rath S, Sharma R, Gupta R, Ast T, Chan C, Durham TJ, et al. MitoCarta3.0: an updated mitochondrial proteome now with sub-organelle localization and pathway annotations. Nucleic Acids Res. 49, D1541–7. (2021).
18. Coleman, R. A., Lewin, T. M., Van Horn, C. G. & Gonzalez-Baró, M. R. Do long-chain acyl-CoA synthetases regulate fatty acid entry into synthetic versus degradative pathways?. *J. Nutr.* **132**, 2123–2126 (2002).
19. Quan, J., Bode, A. M. & Luo, X. ACSL family: The regulatory mechanisms and therapeutic implications in cancer. *Eur. J. Pharmacol.* **909**, 174397 (2021).
20. Padanad, M. S. et al. Fatty Acid Oxidation Mediated by Acyl-CoA Synthetase Long Chain 3 Is Required for Mutant KRAS Lung Tumorigenesis. *Cell. Rep.* **16**, 1614–1628 (2016).
21. Kasuya, F., Tatsuki, T., Ohta, M., Kawai, Y. & Igarashi, K. Purification, characterization, and mass spectrometric sequencing of a medium chain acyl-CoA synthetase from mouse liver mitochondria and comparisons with the homologues of rat and bovine. *Protein. Expr. Purif.* **47**, 405–414 (2006).
22. Fujino, T. et al. Molecular identification and characterization of two medium-chain acyl-CoA synthetases, MACS1 and the Sa gene product. *J. Biol. Chem.* **276**, 35961–35966 (2001).
23. Eleftheriadou M, Medici-van den Herik E, Stuurman K, van Bever Y, Hellebrekers DMEI, van Slegtenhorst M, et al. Isobutyryl-CoA dehydrogenase deficiency associated with autism in a girl without an alternative genetic diagnosis by trio whole exome sequencing: A case report. Mol. Genet. Genomic Med. e1595. (2021).
24. Wanders, R. J. A., Duran, M. & Loupatty, F. J. Enzymology of the branched-chain amino acid oxidation disorders: the valine pathway. *J. Inherit. Metab. Dis.* **35**, 5–12 (2012).
25. Yew, M. J. et al. ACAD10 is not required for metformin's metabolic actions or for maintenance of whole-body metabolism in C57BL/6J mice. *Diabetes Obes. Metab.* **26**, 1731–1745 (2024).
26. Shim, S. M. et al. The Cys-N-degron pathway modulates pexophagy through the N-terminal oxidation and arginylation of ACAD10. *Autophagy* **19**, 1642–1661 (2023).
27. Su, J. et al. Zinc finger nuclease knock-out of NADPH:cytochrome P450 oxidoreductase (POR) in human tumor cell lines demonstrates that hypoxia-activated prodrugs differ in POR dependence. *J. Biol. Chem.* **288**, 37138–37153 (2013).
28. Pillai, V. C., Snyder, R. O., Gumaste, U., Thekkumkara, T. J. & Mehvar, R. Effects of transient overexpression or knockdown of cytochrome P450 reductase on reactive oxygen species generation and hypoxia reoxygenation injury in liver cells. *Clin. Exp. Pharmacol. Physiol.* **38**, 846–853 (2011).
29. Wang, B. et al. Mitochondria are targets for peroxisome-derived oxidative stress in cultured mammalian cells. *Free Radic. Biol. Med.* **65**, 882–894 (2013).
30. Omodei, D., Licastro, D., Salvatore, F., Crosby, S. D. & Fontana, L. Serum from humans on long-term calorie restriction enhances stress resistance in cell culture. *Aging* **5**, 599–606 (2013).
31. Zhang J, Song J, Liu S, Zhang Y, Qiu T, Jiang L, et al. m6A methylation-mediated PGC-1α contributes to ferroptosis via regulating GSTK1 in arsenic-induced hepatic insulin resistance. Science of the Total Environment. 905. (2023).
32. Liu, C. et al. Therapeutic potential and protective role of GRK6 overexpression in pulmonary arterial hypertension. *Vascul Pharmacol.* **153**, 107233 (2023).
33. Chen, X. et al. XBP1 promotes triple-negative breast cancer by controlling the HIF1α pathway. *Nature* **508**, 103–107 (2014).

34. Wise, D. R. et al. Hypoxia promotes isocitrate dehydrogenase-dependent carboxylation of α-ketoglutarate to citrate to support cell growth and viability. *Proc. Natl. Acad. Sci.* **108**, 19611–19616 (2011).
35. Mullen, A. R. et al. Reductive carboxylation supports growth in tumour cells with defective mitochondria. *Nature* **481**, 385–388 (2011).
36. Gaude, E. et al. NADH shuttling couples cytosolic reductive carboxylation of glutamine with glycolysis in cells with mitochondrial dysfunction. *Mol Cell.* **69**, 581-593.e7 (2018).
37. Gameiro, P. A. et al. In vivo HIF-mediated reductive carboxylation is regulated by citrate levels and sensitizes VHL-deficient cells to glutamine deprivation. *Cell Metab.* **17**, 372–385 (2013).
38. Jiang, L. et al. Reductive carboxylation supports redox homeostasis during anchorage-independent growth. *Nature* **532**, 255–258 (2016).
39. Hu, Q. et al. ASS1-mediated reductive carboxylation of cytosolic glutamine confers ferroptosis resistance in cancer cells. *Cancer Res.* **83**, 1646–1665 (2023).
40. Dyer, A. et al. Antagonism of glycolysis and reductive carboxylation of glutamine potentiates activity of oncolytic adenoviruses in cancer cells. *Cancer Res.* **79**, 331–345 (2019).
41. Roma, A., Goodridge, L. D. & Spagnuolo, P. A. Reductive carboxylation of glutamine as a potential target in acute myeloid leukemia. *Oncotarget* **14**, 947–948 (2023).
42. Dai, W. et al. FASN deficiency induces a cytosol-to-mitochondria citrate flux to mitigate detachment-induced oxidative stress. *Cell Rep.* **42**, 112971 (2023).
43. Ji, X. et al. MRPL12-ANT3 interaction involves in acute kidney injury via regulating MPTP of tubular epithelial cells. *Iscience.* **26**, 106656 (2023).
44. Gu, X. et al. Transcription of MRPL12 regulated by Nrf2 contributes to the mitochondrial dysfunction in diabetic kidney disease. *Free Radic. Biol. Med.* **164**, 329–340 (2021).
45. Frei, C., Galloni, M., Hafen, E. & Edgar, B. A. The Drosophila mitochondrial ribosomal protein mRpL12 is required for Cyclin D/Cdk4-driven growth. *EMBO J.* **24**, 623–634 (2005).
46. Ma, Y. et al. SQSTM1/p62 controls mtDNA expression and participates in mitochondrial energetic adaption via MRPL12. *Iscience.* **23**, 101428 (2020).
47. Koehn, O. J. et al. GTPase splice variants RAC1 and RAC1B display isoform-specific differences in localization, prenylation, and interaction with the chaperone protein SmgGDS. *J. Biol. Chem.* **299**, 104698 (2023).
48. Tew, G. W. et al. SmgGDS regulates cell proliferation, migration, and NF-kappaB transcriptional activity in non-small cell lung carcinoma. *J. Biol. Chem.* **283**, 963–976 (2008).
49. Kudo, S. et al. SmgGDS as a crucial mediator of the inhibitory effects of statins on cardiac hypertrophy and fibrosis: Novel mechanism of the pleiotropic effects of statins. *Hypertension* **67**, 878–889 (2016).
50. Song, H. et al. Selective autophagy receptor NBR1 retards nucleus pulposus cell senescence by directing the clearance of SRBD1. *Int. J. Biol. Sci.* **20**, 701–717 (2024).
51. Oji, Y. et al. Variants in saposin D domain of prosaposin gene linked to Parkinson's disease. *Brain* **143**, 1190–1205 (2020).
52. Sun, Y., Qi, X. & Grabowski, G. A. Saposin C is required for normal resistance of acid beta-glucosidase to proteolytic degradation. *J. Biol. Chem.* **278**, 31918–31923 (2003).
53. Chatelut, M. et al. Model SV40-transformed fibroblast lines for metabolic studies of human prosaposin and acid ceramidase deficiencies. *Clin. Chim. Acta.* **262**, 61–76 (1997).
54. Henseler, M., Klein, A., Glombitza, G. J., Suziki, K. & Sandhoff, K. Expression of the three alternative forms of the sphingolipid activator protein precursor in baby hamster kidney cells and functional assays in a cell culture system. *J. Biol. Chem.* **271**, 8416–8423 (1996).
55. Hamada, N. et al. Anti-vascular endothelial growth factor gene therapy attenuates lung injury and fibrosis in mice. *J. Immunol.* **175**, 1224–1231 (2005).
56. Bueno M, Lai Y-C, Romero Y, Brands J, St Croix CM, Kamga C, et al. PINK1 deficiency impairs mitochondrial homeostasis and promotes lung fibrosis. J. Clin. Investig.. 125. (2015).
57. Aquino-Gálvez, A. et al. Dysregulated expression of hypoxia-inducible factors augments myofibroblasts differentiation in idiopathic pulmonary fibrosis. *Respir Res.* **20**, 130 (2019).
58. Tian, G. et al. Voltage-dependent anion channel 1 (VDAC1) overexpression alleviates cardiac fibroblast activation in cardiac fibrosis via regulating fatty acid metabolism. *Redox Biol.* **67**, 102907 (2023).
59. Raghu, G., Weycker, D., Edelsberg, J., Bradford, W. Z. & Oster, G. Incidence and prevalence of idiopathic pulmonary fibrosis. *Am. J. Respir. Crit. Care Med.* **174**, 810–816 (2006).
60. Fell, C. D. et al. Clinical predictors of a diagnosis of idiopathic pulmonary fibrosis. *Am. J. Respir. Crit. Care Med.* **181**, 832–837 (2010).
61. Kirkwood, T. B. L. & Kowald, A. The free-radical theory of ageing–older, wiser and still alive: modelling positional effects of the primary targets of ROS reveals new support. *BioEssays* **34**, 692–700 (2012).
62. Park, C. B. & Larsson, N.-G. Mitochondrial DNA mutations in disease and aging. *J. Cell. Biol.* **193**, 809–818 (2011).
63. Moskalev, A. A. et al. The role of DNA damage and repair in aging through the prism of Koch-like criteria. *Ageing Res. Rev.* **12**, 661–684 (2013).
64. Zhao, Y. D. et al. Metabolic heterogeneity of idiopathic pulmonary fibrosis: a metabolomic study. *BMJ Open Respir. Res.* **4**, e000183 (2017).
65. Kottmann, R. M. et al. Lactic acid is elevated in idiopathic pulmonary fibrosis and induces myofibroblast differentiation via pH-dependent activation of transforming growth factor-β. *Am. J. Respir. Crit. Care Med.* **186**, 740–751 (2012).
66. Hecker, L. et al. NADPH oxidase-4 mediates myofibroblast activation and fibrogenic responses to lung injury. *Nat. Med.* **15**, 1077–1081 (2009).
67. Wiśniewska, A. et al. Diminished toxicity of C-1748. *Biochem. Pharmacol.* **84**, 30–42 (2012).
68. Osada, M., Imaoka, S., Sugimoto, T., Hiroi, T. & Funae, Y. NADPH-cytochrome P-450 reductase in the plasma membrane modulates the activation of hypoxia-inducible factor 1. *J. Biol. Chem.* **277**, 23367–23373 (2002).
69. Zhou, T.-B., Qin, Y.-H., Lei, F.-Y., Huang, W.-F. & Drummen, G. P. C. Association of prohibitin-1 and 2 with oxidative stress in rats with renal interstitial fibrosis. *Mol. Biol. Rep.* **41**, 3033–3043 (2014).
70. Xu, Q. et al. Hypoxia regulation of ATP13A2 (PARK9) gene transcription. *J. Neurochem.* **122**, 251–259 (2012).
71. Rajagopalan, S., Rane, A., Chinta, S. J. & Andersen, J. K. Regulation of ATP13A2 via PHD2-HIF1α signaling is critical for cellular iron homeostasis: Implications for Parkinson's disease. *J. Neurosci.* **36**, 1086–1095 (2016).
72. Hamanaka, R. B. et al. Glutamine metabolism is required for collagen protein synthesis in lung fibroblasts. *Am. J. Respir. Cell. Mol. Biol.* **61**, 597–606 (2019).
73. Bernard, K. et al. Glutaminolysis is required for transforming growth factor-β1-induced myofibroblast differentiation and activation. *J Biol. Chem.* **293**, 1218–1228 (2018).
74. Ge, J. et al. Glutaminolysis promotes collagen translation and stability via. *Am J Respir. Cell. Mol. Biol.* **58**, 378–390 (2018).

Acknowledgements

Arnoldo Aquino-Gálvez and Yair Romero would like to thank Dr. Moisés Selman for his support and various

stages of this project. Mass spectrometry-based proteomics was performed at the Genomics, Proteomics and Metabolomics Core Facility (UGPM), LaNSE, Cinestav Zacatenco; hence, we want to thank ChemE, Nataly Ramos Buendía, for her help during sample preparation for proteomics analysis.

Author contributions

A. A.-G. conceptualized the idea, secured funding, designed experiments, coordinated the entire project, and wrote the manuscript. Y. R. designed and coordinated most experiments, also contributing to the manuscript's writing. R. V.-C. designed experiments, critically reviewed the writing, helped secure economic resources, and coordinated the proteomics section. E. R. L.-G. performed mitochondria purification, protein extraction, and Western blots. I. H. and C. B. were responsible for cell line care and propagation, collaborating on specific experiments. A. B.-C. carried out all bioinformatics analysis of proteomic data. D. I. A.-B. participated in protein quantification, integrity gels for proteomics, and select experiments. E. R.-C. performed the proteomic analysis with the team and coordinated the overall proteomics section. N. T.-R. and R. O.-H. obtained electron microscopy images to validate mitochondria purification. A. K. T.-S., a graduate student, participated in cell line care and culture. M. C.-L. guided and revised the statistical analysis and critically reviewed the writing and grammar. V. R., J. C., J. Z., E. F.-S., Y. I. B.-M., Á. C.-R., and L. M. T.-E. collaborated on experimental execution and provided critical review of the manuscript, with Y. I. B.-M. also supporting figure preparation.

Funding

This work was fully funded by the Consejo Nacional de Humanidades Ciencia y Tecnología (CONAHCYT CIENCIA DE FRONTERA 2019), entitled "Proteomic analysis of mitochondria from healthy and fibrotic lung fibroblasts exposed to hypoxia," F/3578; Project 194162. Ana Karen Torres Soria, as a student of the Master's at the Escuela Superior de Medicina del Instituto Politécnico Nacional (IPN), received the CVU 1095773 scholarship from CONAHCYT and Physician Angélica Varela Ordoñez received financial support at the undergraduate level from CONAHCYT Project 194162.

Declarations

Competing interests

The authors declare no competing interests.

Ethical approval

This study was approved by all institutional research committees, including the ethics committee of the Instituto Nacional de Enfermedades Respiratorias Ismael Cosío Villegas (INER), and was registered under number B02-19.

Additional information

Supplementary Information The online version contains supplementary material available at https://doi.org/10.1038/s41598-025-26911-3.

Correspondence and requests for materials should be addressed to R.V.-C. or A.A.-G.